A Novel CMOS High-Power Terahertz VCO Based on Coupled Oscillators: Theory and Implementation

Yahya M. Tousi, *Member, IEEE*, Omeed Momeni, *Member, IEEE*, and Ehsan Afshari, *Senior Member, IEEE*

***Abstract*—We introduce a novel frequency tuning method for high-power terahertz sources in CMOS. In this technique, multiple core oscillators are coupled to generate, combine, and deliver their harmonic power to the output node without using varactors. By exploiting the theory of nonlinear dynamics, we control the coupling between the cores to set their phase shift and frequency. Using this method, two high-power terahertz VCOs are fabricated in a 65 nm LP bulk CMOS process. The first one has a measured output power of 0.76 mW at 290 GHz with 4.5% tuning range and the output power of the second VCO is 0.46 mW at 320 GHz with 2.6% tuning range. The output power of these signal sources is 4 orders of magnitude higher than previous CMOS VCOs and is even higher than VCOs implemented in compound semiconductors with much higher cut-off frequencies.**

***Index Terms*—CMOS, coupled oscillator, distributed systems, frequency tuning, harmonic generation, matching, nonlinear dynamics, power combining, phase shifter, Terahertz, VCO.**

I. Introduction

THE last few years have witnessed a surge in mm-wave integrated circuits mainly because of the increased cut-off frequency of CMOS transistors. These integrated systems target applications such as wide-band communication, remote sensing, and medical imaging [1]–[12]. Moreover, recent works have shown the possibility of implementing CMOS circuits at sub-mm-wave and terahertz frequencies defined from 300 GHz to 3 THz. This is motivated by the higher communication bandwidth and better imaging resolution in addition to new applications such as integrated terahertz spectroscopy [11]–[19]. Despite all recent advances in this frequency range, a high-power tunable signal source has remained a challenging yet essential circuit block toward the realization of a complete terahertz system.

In LC-resonator-based voltage-controlled oscillators (VCO), varactors are placed in the resonator in order to tune the oscillating frequency. This tuning method works well at radio frequencies and achieves moderate tunability at lower mm-wave frequencies ($<$100 GHz) [2]–[4]. However, there are at least two major challenges in using varactors for frequency tuning above 100 GHz. First, at these frequencies the varactor quality factor is low. This lowers the achievable output power and degrades the phase noise performance. Secondly, as the operation frequency increases, the parasitic capacitances dominate the tank, limiting the tuning capability of varactors. These challenges impose an important trade-off in the design of high frequency oscillators. CMOS oscillators above 100 GHz with high output power, do not use varactors and as a result their frequency cannot be tuned [13], [14]. On the other hand, tunable oscillators at these frequencies provide very low output powers (<1 μW) due to the use of tuning varactors [15], [16]. As a result of these challenges, power generation along with frequency tuning above 150 GHz is dominated by frequency multipliers [19]–[21]. Frequency multiplication requires a high-power external source which is not desirable in a fully integrated terahertz source.

To address this challenge, prior works at lower frequencies have focused on tuning the oscillation frequency without using varactors [22]–[24]. The magnetically-tuned and the transconductance-tuned VCOs are two examples where instead of capacitive tuning, the effective inductor of the tank is tuned. Both of these techniques still require additional active devices inside the oscillator tank. A recent work has used an interpolative-phase-tuning technique in an LC ring oscillator at the mm-wave frequency range [25]. All these techniques have been used to generate output powers well below the cut-off frequency of the transistors.

In order to realize a high-power VCO at the sub-mm-wave and terahertz band, three requirements need to be satisfied: First, the signal source should be able to generate high harmonic power above the device $f_{\max}$. Second, the generated power should be efficiently delivered to the output load. Third, a frequency tuning mechanism should be proposed that would not adversely affect the first two requirements.

In this work we introduce a novel VCO architecture based on coupled oscillators in a loop configuration that is suitable for terahertz power generation. We show that because of the new approach to frequency control, the trade-off between frequency tuning and power generation in conventional VCOs is largely resolved. As a result, frequency tuning is achieved while maintaining high output power in the sub-mm-wave frequency range. Furthermore, the proposed technique provides an effective way to generate and combine the harmonics of the fundamental frequency from multiple core oscillators. Using a standard low-power 65 nm CMOS process, we demonstrate a 290 GHz VCO with 0.76 mW (-1.2 dBm) output power and 13 GHz tuning range and a 320 GHz VCO with 0.46 mW (-3.3 dBm) output

Manuscript received April 22, 2012; revised June 26, 2012; accepted July 16, 2012. Date of publication October 19, 2012; date of current version December 21, 2012. This paper was approved by Guest Editor Pietro Andreani.

Y. M. Tousi and E. Afshari are with Cornell University, Ithaca, NY 14853 USA (e-mail: ym225@cornell.edu).

O. Momeni is with the Department of Electrical and Computer Engineering, University of California at Davis, Davis, CA 95616-5294 USA.

Color versions of one or more of the figures in this paper are available online at http://ieeexplore.ieee.org.

Digital Object Identifier 10.1109/JSSC.2012.2217853

power and 8.4 GHz tuning range [26]. These VCOs achieve the highest output power among all reported CMOS VCOs as well as compound semiconductor VCOs around 300 GHz.

The rest of the paper is organized as follows. Section II describes the theory of the proposed coupled oscillator system, Section III explains the VCO architecture and Section IV describes the implementation and measurement results. Finally, Section V concludes the paper.

II. Theory of Coupled Oscillators

The dynamics of interaction between two electrical oscillators has been studied by Adler in the context of injection locking [27]. Based on this analysis, when an oscillator at ω_1 injects energy to another one with a free-running oscillation frequency of ω_0, under locking conditions, the second oscillator follows the first with an equal frequency and a phase shift of

$$\Delta\phi = \sin^{-1}\left(2Q\frac{I_{\rm core}}{I_{\rm inj}}\cdot\frac{\Delta\omega}{\omega_0}\right) \tag{1}$$

where $\Delta\phi$ is the phase difference developed as a result of the frequency difference $\Delta\omega = \omega_1 - \omega_0$. In (1), Q represents the quality factor of the resonator and $I_{\rm core}$ and $I_{\rm inj}$ are the currents delivered to the resonator from its active element and the injecting source, respectively.

The above relation also yields the locking range by finding the frequency difference $\Delta\omega$ at which $|\Delta\phi| = \pi/2$. As (1) implies, lowering the quality factor and/or increasing the amplitude of the injected signal results in a wider locking range.

The lower and upper bounds of the locking range are derived by finding the frequencies where the phase shift equals to $-\pi/2$ and $\pi/2$, respectively. Intuitively, at these frequencies the in-phase component of the injected signal disappears and as a result, the injected signal has no effect on the dynamics of the main oscillator. This frequency locking phenomena has been applied to electrical oscillators for applications including frequency division, coupled radiation systems, and beam-steering [28]–[34]. The main similarity between all these systems is that there is an external signal source and one or more oscillators are coupled and eventually synchronized to that external source.

Coupled systems do not necessarily need an external source and can rely on internal couplings to synchronize. A study by York exploits passive mutual coupling between an array of oscillators to synchronize them in order to facilitate spatial power combining [35]. In general, the method of coupling and its dynamics as well as the geometry of the coupled system can be engineered for a diverse range of functionalities. In this work, we propose a particular coupling topology between N core oscillators that controls the frequency of the oscillators and imposes a constant desired phase shift between them. As we show later, this constant phase shift is critical in harmonic power combining from core oscillators.

A. Actively Coupled Oscillators

An insightful observation from (1) suggests that while a phase shift is developed as a result of the frequency difference between the cores, the reverse phenomena is also possible. In a system of coupled oscillators, if the phase shift between the the injected signal and the main oscillator is changed, the locking frequency is forced to change. In the conventional locking scheme this cannot happen because the frequency of the injecting signal is fixed and the phase difference is dictated by (1). In contrast, in a coupling scheme that only relies on internal couplings, the locking frequency is determined based on internal parameters of the system. The scheme in Fig. 1 shows a ring of N coupled oscillators. In this architecture, the ith oscillator injects energy to the $(i+1)$th oscillator while receiving energy from the $(i-1)$th oscillator. The coupling between the consecutive cores is performed by a tunable phase shift.

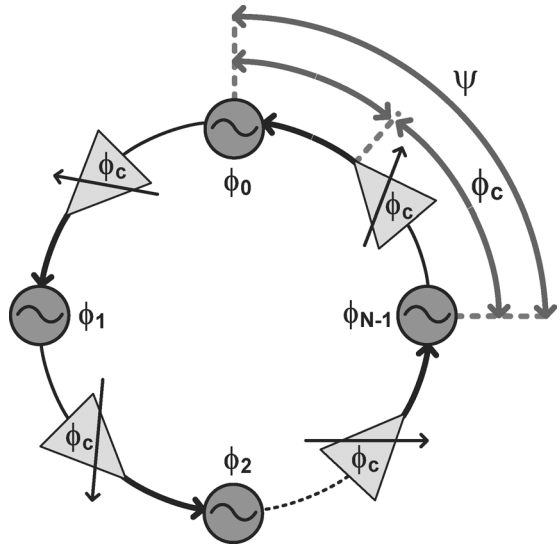

Fig. 1. A loop structure consisting of N coupled oscillators.

In order to analyze the dynamics of this system, we assume sinusoidal coupling between the adjacent cores which is a good approximation close the the resonance frequency [27]. Under this assumption, if ϕ_i is the rotating phase of the ith oscillator and all cores have a similar free running oscillating frequency of ω_0, the phase dynamics can be described by

$$\dot{\phi_i} = \omega_0 + K\sin(\phi_{i-1} + \phi_c - \phi_i) \tag{2}$$

where $K = (I_{\rm inj})/(I_{\rm core})(\omega_0)/(2Q)$ is the coupling factor and ϕ_c is the phase shift resulting from the coupling block. In this scheme all phase shifts are assumed to be equal.

By defining $\psi_i = \phi_i - \phi_{i-1}$ as the instantaneous phase shift between the adjacent oscillators, we can rewrite the set of equations described by (2) as

$$\dot{\psi_i} = K\sin(\phi_c - \psi_i) - K\sin(\phi_c - \psi_{i-1}). \tag{3}$$

This relation describes the dynamics of ψ_i, the phase difference between adjacent cores in the ring. For the complete description of the dynamics, the boundary condition from the loop should be included. The total phase shift around the loop is fixed:

$$\sum_i \psi_i = 2k\pi \tag{4}$$

where k is an integer. The solution to the above set of differential equations describes the phase dynamics of the system, which also results in the stable solutions.

B. Stability Analysis

A steady state solution to (3) is determined by finding the phase shifts that satisfy $\dot{\psi}_i = 0$. From (3) the solutions for each differential equation can be either $\Psi_i = \Psi_{i-1}$ or $\Psi_i = 2\phi_c - \pi - \Psi_{i-1}$, where Ψ is the steady-state solution of ψ for all N differential equations. However, it can be shown [36] that the loop condition (4) is satisfied for all values of ϕ_c, only when

$$\Psi_i = \Psi_{i-1} = \Psi. \tag{5}$$

Furthermore, for this solution to be stable a small perturbation must attenuate in time and bring the system back to its original state. By applying a perturbation of η_i to this solution we have

$$\psi_i = \Psi + \eta_i. \tag{6}$$

By replacing (6) into (3) the dynamics of the perturbed system is derived:

$$\dot{\eta_i} = K\sin(\phi_c - \Psi - \eta_i) - K\sin(\phi_c - \Psi - \eta_{i-1}) \tag{7}$$

and for a small perturbation around the solution and by substituting (3) for $\dot{\psi}_i = 0$, (7) becomes

$$\dot{\eta_i} \simeq K\cos(\phi_c - \Psi)\eta_{i-1} - K\cos(\phi_c - \Psi)\eta_i. \tag{8}$$

This results in a set of linear differential equations in the form of

$$\dot{H} = A \cdot H \tag{9}$$

where H is a vector with $H_i = \eta_i$ and A is an $N \times N$ matrix with values $A_{i,i} = -K\cos(\phi_c - \Psi)$, $A_{i,i-1} = K\cos(\phi_c - \Psi)$, and zero for the rest of the elements.

A necessary condition for stability is that all eigenvalues of A are non-positive [37]. It can be shown that A has N separate eigenvalues with values of

$$\lambda_i = K\cos(\phi_c - \Psi) \cdot \left(e^{j2\pi i/N} - 1\right) \tag{10}$$

where $0 \leq i < N$. Here K is positive and the term inside the bracket is less or equal to zero when $\cos(\phi_c - \Psi) \geq 0$. This means

$$\phi_c - \pi/2 \leq \Psi \leq \phi_c + \pi/2. \tag{11}$$

For values inside this boundary, λ_1 to λ_{N-1} are negative and as a result, the response of the system to a small perturbation diminishes. Consequently the coupled system is stable under the conditions in (11).

The solutions to this system of differential equations are values of Ψ that satisfy (4). This results in

$$\Psi_k = 2k\pi/N \tag{12}$$

where k is an integer representing N different solutions. These solutions are the N possible coupling modes in the coupled oscillator system. The stable region for the kth coupling mode corresponding to Ψ_k is found by replacing (12) into (11):

$$\Psi_k - \pi/2 \leq \phi_c \leq \Psi_k + \pi/2. \tag{13}$$

Fig. 2 shows the stable regions as a function of the phase shift ϕ_c. Interestingly, there are more than one stable solution for a given phase shift and depending on the initial conditions the system settles to one of the modes. However, based on our analysis as long as the system in a particular mode satisfies (13), it remains in that mode.

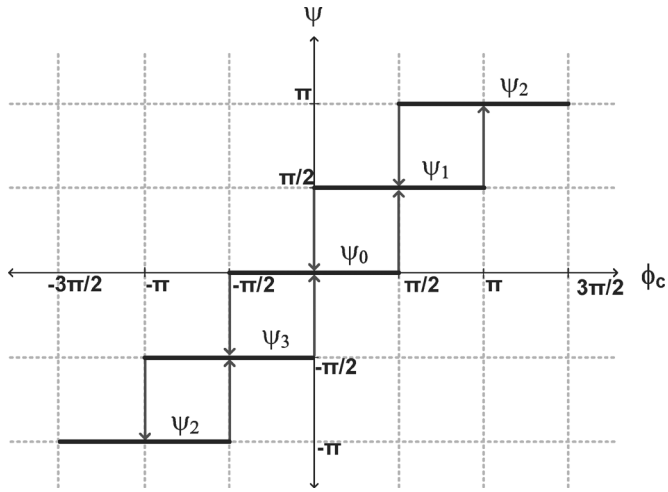

Fig. 2. Stable regions for different modes of a system of four coupled oscillators.

If the phase shift is changed beyond the stable conditions of the current mode, the system becomes unstable and moves out of this mode toward a stable mode. The transition from one mode to the other mode can be described by the general nonlinear differential equations of (2). Using the theory of nonlinear dynamics, it can be shown that for $N = 4$ the system settles to the directly next state in the diagram of Fig. 2 [36]. This means that for a stable solution at Ψ_k, increasing ϕ_c eventually moves the system into Ψ_{k+1}, which is the next stable mode. Similarly, reducing ϕ_c moves the system into Ψ_{k-1}. During this transition the phase difference ψ_i gradually increases (or decreases) and finally settles to the next stable mode. This behavior can be seen in Fig. 3 for a system with 4 coupled oscillators. A small step in ϕ_c moves the system one step up to the next mode or one step down to the prior mode.

A useful feature of this actively coupled oscillator scheme is its ability to deliberately select any desired mode. As shown in Fig. 2 for a given ϕ_c, the system can settle to one out of a few modes depending on the initial conditions. However, by changing ϕ_c in a deterministic way, a particular mode can be selected. After choosing this mode, the hysteresis in the system keeps the system in that mode as long as the stability conditions are satisfied. This is in contrast to the quadrature oscillators where a phase uncertainty is inherent to the system. We can consider the quadrature oscillator a special case of this coupled system for $N = 2$, resulting in two stable modes at $\Psi = \pi/2$ and $\Psi = -\pi/2$. Without the tunable phase shifters, for $\phi_c = 0$ the system randomly chooses either of the coupling modes resulting in ambiguity in the locking frequency [38].

C. Frequency Tuning

When the coupled oscillators are locked together at the kth coupling mode, by substituting $\Psi_k = \phi_i - \phi_{i-1}$ into (2), the frequency of all core oscillators, ω becomes

$$\omega = \omega_0 + K\sin(\phi_c - \Psi_k). \tag{14}$$

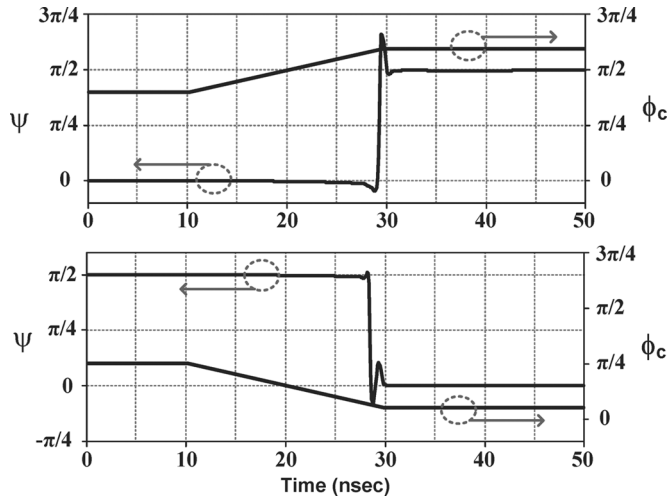

Fig. 3. Mode transition in the system of 4 coupled oscillators. Top: Transition from $\Psi = 0$ to $\Psi = \pi/2$. Bottom: Transition from $\Psi = \pi/2$ to $\Psi = 0$.

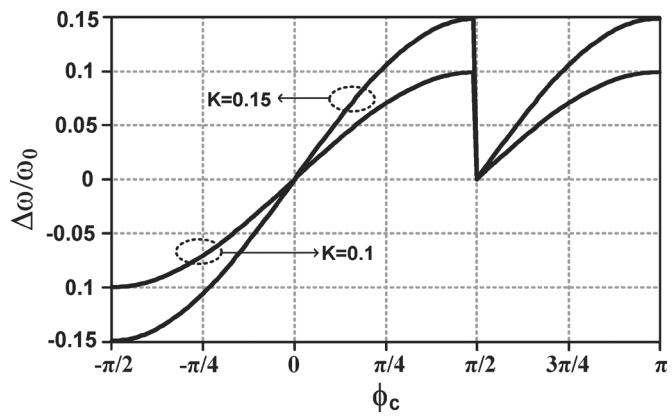

Fig. 4. Relative frequency as a function of ϕ_c for two values of K. The jump in the output frequency corresponds to the change in the coupling mode from $\Psi = 0$ to $\Psi = \pi/2$.

Note that from (13), $\phi_c - \Psi_k$ is always between $-\pi/2$ and $\pi/2$ in the stable region of any given coupling mode. When the amount of phase shift exceeds the stability limit of the operating mode, the coupling mode changes to the next mode resulting in an abrupt step in the output frequency as shown in Fig. 4.

By substituting for K in (14), the frequency tuning range is equal to

$$\frac{\Delta\omega}{\omega_0} = \pm\frac{1}{2Q}\cdot\frac{I_{\text{inj}}}{I_{\text{core}}}. \tag{15}$$

This tuning range can be increased by increasing the coupling factor. Since reducing Q is not desirable for the purpose of harmonic power generation and low phase-noise, the best way to increase the tuning range is by increasing I_{inj}.

III. Terahertz Harmonic VCO

We exploit the frequency tuning concept of the actively coupled oscillator structure for generation of high-power and tunable signal sources around 300 GHz. In order to generate power above the transistor $f_{\max}$, we employ harmonic generation. The generated harmonic power should be maximized and optimally delivered to the output node. Prior work has been able to produce $>100\ \mu$W of output power on silicon at sub-mm-wave frequencies by optimizing the device embedding for efficient generation and delivery of the harmonic power to the load [13]. For such a design, a reasonable quality factor is required in the signal path which is only possible by avoiding varactors. This limits the oscillator to a single frequency. Our proposed structure provides an effective method to tune the frequency while maintaining the high output power.

First, the oscillator core is optimized to generate the highest possible power at the harmonic of the fundamental frequency. Then, four cores are coupled and the generated powers from all cores are combined and delivered to the load. In addition to harmonic generation, the coupling dynamic performs two tasks: (1) it determines the coupling mode and (2) in that given mode it controls the operating frequency of the core oscillators. The coupling circuits (i.e., phase shifters) operate at the fundamental frequency and are buffered from the cores. Hence, the tasks of power generation and frequency tuning are separated, resulting in a high-power tunable source.

A. Oscillator Design

For a given target frequency at a given technology, the first design step is to find the best harmonic of the fundamental to use as the output frequency. The advantage of using a higher harmonic number is that the fundamental frequency is lower and generates larger amplitudes, resulting in more nonlinearity. However, the power generated at higher harmonics is significantly smaller than lower harmonics. On the other hand, using lower harmonic numbers forces the fundamental frequency to become close to $f_{\max}$, resulting in a low fundamental power to begin with. As a result, there is a trade-off in choosing the harmonic number and the lowest harmonic number is not necessarily the best choice.

In this design, for a target frequency of 300 GHz, the fourth harmonic is chosen for the highest power generation. The simulated $f_{\max}$ of this process in around 200 GHz and as a result, using the second harmonic results in a fundamental of 150 GHz which is too close to $f_{\max}$. As shown in Fig. 5, the fourth harmonic generates a higher harmonic current compared to the second harmonic. This is mainly because of the larger nonlinearity produced by a fundamental frequency around 75 GHz. As simulations indicate, the third harmonic creates slightly higher levels of harmonic current. However, in this design even harmonics are favored because of the resulting symmetry in implementation of the coupled system. By using the fourth harmonic in this design, the cross-coupled LC oscillator can be used as the core oscillator.

The LC resonator design should result in optimum performance both at the fundamental and the fourth harmonic. Consider the circuit in Fig. 6, where the conventional cross coupled structure is extended into a more general resonator. The fundamental frequency is determined by the resonance frequency of the network. Moreover, at the fourth harmonic the network has to deliver maximum power from the transistor to the load. Both

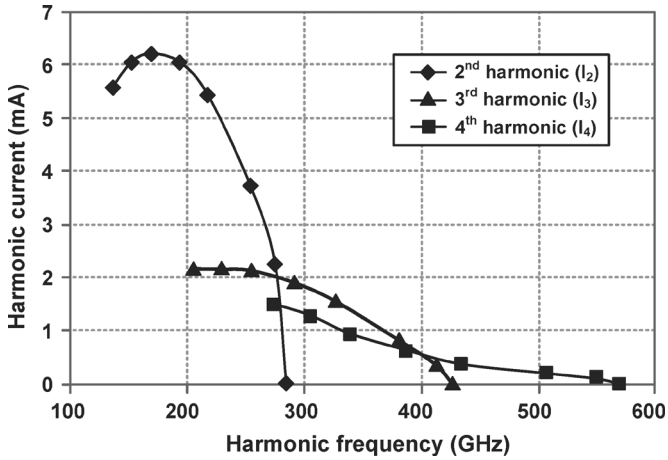

Fig. 5. Simualted harmonic current generated at the drain of a 65 nm CMOS transistor in a basic cross-coupled oscillation scheme.

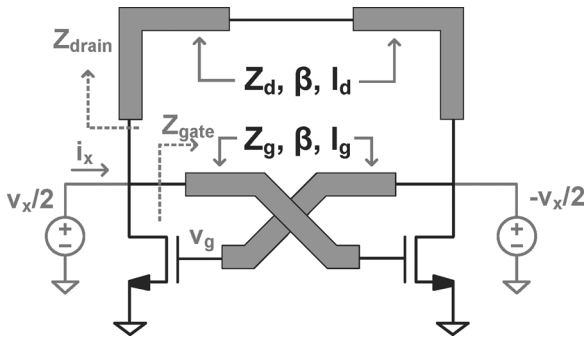

Fig. 6. The modified cross-coupled scheme employed and the equivalent circuit at the fundamental frequency.

the fundamental frequency and maximum harmonic power delivery can be simultaneously achieved by adding an impedance to the gate of the transistor. For practical purposes we employ two transmission lines for the gate and drain lines. Let us assume the gate and drain lines have characteristic impedances of Z_g and Z_d with lengths of l_g and l_d, respectively. For this analysis, we model the transistor only with the gate capacitance C_g and a transconductance of g_m.

The equivalent circuit of the cross-coupled pair at the fundamental frequency is shown in Fig. 6. To find the impedance of the resonator, we write the governing equation at the output node. By applying a differential voltage source v_x, the resulting current i_x equals to:

$$i_x = g_m v_g + \frac{v_x}{2Z_{\rm gate}} + \frac{v_x}{2Z_{\rm drain}} \tag{16}$$

where v_g is the voltage at the gate, and $Z_{\rm gate}$ and $Z_{\rm drain}$ are the impedances looking into the gate and drain lines respectively. By calculating $Z_{\rm gate}$, $Z_{\rm drain}$ and v_g using transmission line analysis the resonator transconductance, G_m can be derived [39]:

$$G_m = \frac{i_x}{v_x} = -\frac{g_m}{2}\cdot\frac{1+\Gamma}{e^{j\beta l_g}+\Gamma e^{-j\beta l_g}} + \frac{1}{2Z_g}\cdot\frac{1-\Gamma e^{-j2\beta l_g}}{1+\Gamma e^{-j2\beta l_g}} + \frac{1}{2Z_d}\cdot\frac{1+e^{-j2\beta\, l_d}}{1-e^{-j2\beta\, l_d}} \tag{17}$$

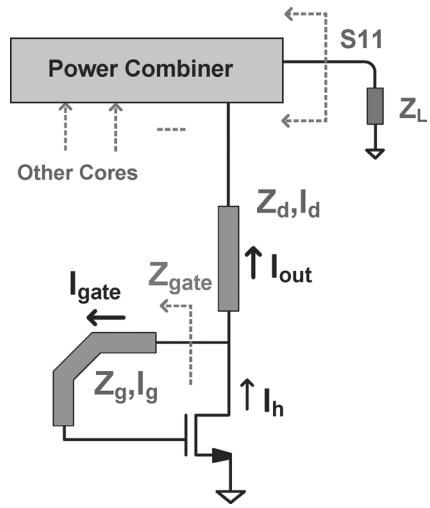

Fig. 7. Half-circuit equivalent of the core oscillator at the fourth harmonic frequency.

where Γ is the reflection coefficient at the gate of the transistor and β is the propagation constant. While this analysis neglects the effect of loss of the lines and the transistor, it is helpful for finding the resonance frequency. In this design, l_g and l_d are significantly smaller than the wavelength at the fundamental frequency of 75 GHz, or equivalently $\beta l_g \ll 1$ and $\beta l_d \ll 1$. By applying these approximations and substituting for Γ, (17) can be simplified as

$$G_m \simeq -\frac{g_m}{2} + \frac{jC_g\omega}{2} + \frac{1}{2Z_d\cdot j\beta\, l_d}. \tag{18}$$

This suggests that in the proposed oscillator, the gate transmission line has minimal effect on the fundamental frequency. This frequency, ω_0 can be calculated by setting the imaginary part of G_m equal to zero:

$$\omega_0 = \sqrt{\frac{v_p}{C_g Z_d l_d}} \tag{19}$$

where $v_p = \omega/\beta$ is the propagation velocity of the wave in silicon dioxide.

B. Harmonic Power Generation

At the fourth harmonic, the cross-coupled pair operates in common mode resulting in a half-circuit equivalent shown in Fig. 7. Nonlinearity of the device generates a harmonic current I_h at the drain of the transistor. For the highest power delivery this current has to be optimally delivered to the load.

As shown in Fig. 7, I_h is divided into the two branches, $I_{\rm out}$ which proceeds to the output load and $I_{\rm gate}$ which returns to the gate of the transistor. To maximize the output power, I_h should flow to the output node which means $Z_{\rm gate}$ has to be maximum at the fourth harmonic to minimize $I_{\rm gate}$. By using an analysis similar to Section III.A, the gate impedance equals to:

$$Z_{\rm gate} = \frac{1}{2Z_g}\cdot\frac{1-\Gamma e^{-j2\beta l_g}}{1+\Gamma e^{-j2\beta l_g}}. \tag{20}$$

$Z_{\rm gate}$ is maximum at its resonance frequency. By proper design of l_g and Z_g, this resonance is placed around the fourth harmonic.

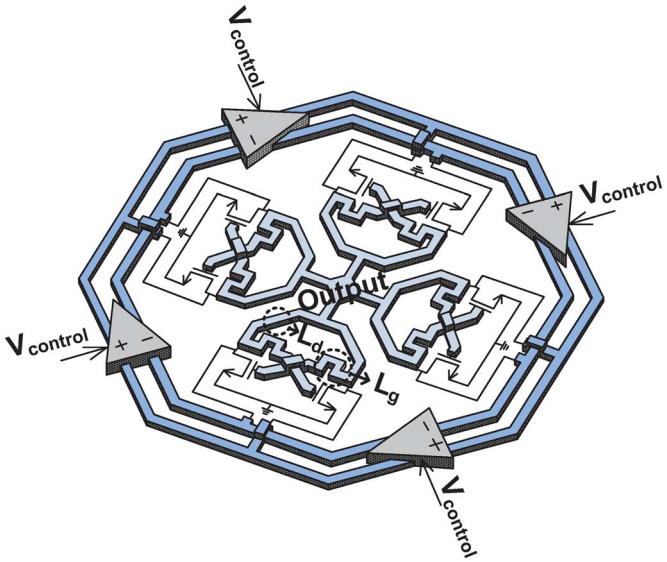

Fig. 8. Top view of the proposed four core coupled oscillator VCO showing the cores, the coupling block, and the power combiner.

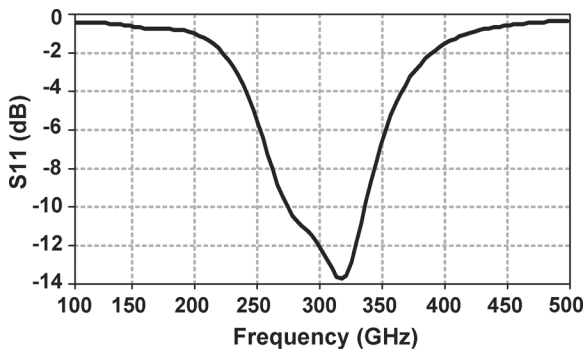

Fig. 9. Simulated output matching of the oscillator at the fourth harmonic.

The output of the four cores are connected to a power combiner. To design a VCO at the fourth harmonic, the coupling mode is set for $\Psi = \pi/2$. In this mode the second harmonic from the four cores cancel out at the output. The first and third harmonics are also canceled because of the differential structure. As a result, the lowest harmonic frequency at the output is the fourth harmonic. Furthermore, for optimal power combining, the drain impedance of the transistor has to be power matched. The VCO including the four coupled cores and the combining network is shown in Fig. 8. The drain lines are first connected together and subsequently connected to the load. The impedance and length of the lines are designed for matching at the fourth harmonic. The resulting output matching is shown in Fig. 9. Fig. 10 shows the waveforms of the core oscillators at the fundamental frequency and the output node at the fourth harmonic.

C. Coupling

As explained in Section II, the coupling block requires a tunable phase shifter in order to control the frequency and the coupling mode. Besides, this block should be buffered from the core oscillators to minimize the power loss due to coupling. Fig. 11 shows the designed coupling network. The circuit consists of

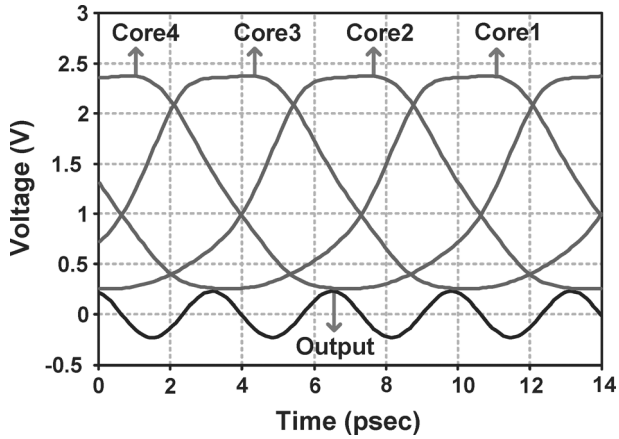

Fig. 10. Simulated waveforms of the core oscillators and the output node, oscillating at the fourth harmonic frequency.

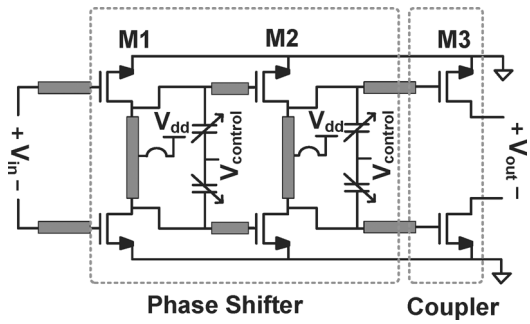

Fig. 11. The differential phase shifter followed by the coupler to the next core.

three stages. The first two stages composed of transistors M1 and M2 act as variable phase shifters and the third stage, M3, acts as a buffer prior to connecting the phase shifters to the next core oscillator. A fully differential scheme is implemented and the supply of the phase shifters is provided through the virtual ground.

The two stage phase shifter is composed of two resonating amplifiers. The resonance frequency is designed to be close to the fundamental frequency of the core oscillators. The varactor tunes the resonance frequency and subsequently changes the overall phase shift. To better understand the process, let us consider the resonator at frequencies close to the resonance frequency [27]. It can be shown that the total phase shift of the phase shifter is

$$\phi_c(\omega) = \phi_c^o + \frac{4Q_c}{\omega_r} \cdot (\omega - \omega_r) \tag{21}$$

where ω_r and Q_c are the center frequency and quality factor of each resonator, respectively. ϕ_c^o represents the phase shift at $\omega = \omega_r$ from the output of the prior core to the injecting current from M3 to the next core. The total phase shift ϕ_c includes the variable phase shifts from the first the two stages and the fixed phase shift from M3.

In order to find the resulting frequency, we place (21) into the coupling equation in (14):

$$\omega = \omega_0 + K \sin\left(\phi_c^o + \frac{4Q_c}{\omega_r} \cdot (\omega - \omega_r) - \Psi_k\right). \tag{22}$$

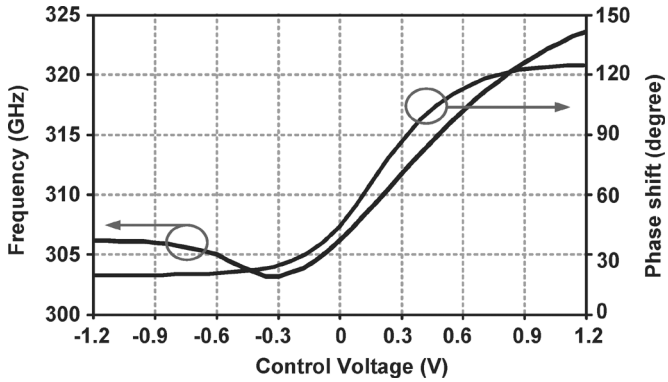

Fig. 12. Simulated phase shift of the coupling block with respect to the control voltage and the resulting change in the locking frequency of the core oscillators.

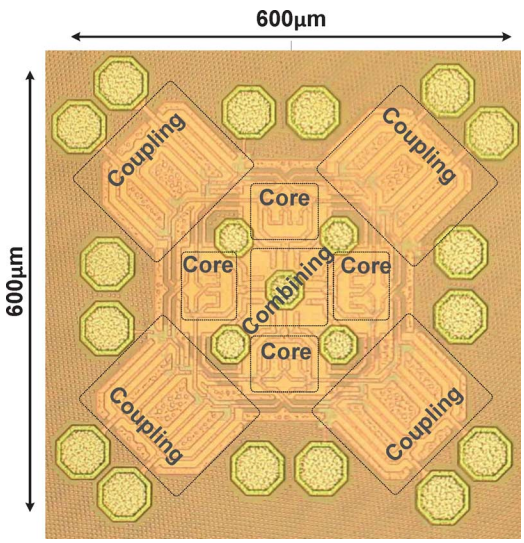

Fig. 13. The chip microphotograph.

Finding the exact tuning range requires numerical simulation. However, it is instructive to find the trend in (22) by finding the change in the oscillating frequency with respect to ω_r:

$$\frac{d\omega}{d\omega_r} = \frac{-\frac{4KQ_c}{\omega_r^2}\omega\cos\left(\phi_c^o - \Psi_k + \frac{4Q_c}{\omega_r}(\omega-\omega_r)\right)}{1-\frac{4KQ_c}{\omega_r}\cos\left(\phi_c^o - \Psi_k + \frac{4Q_c}{\omega_r}(\omega-\omega_r)\right)}. \quad (23)$$

The tuning method is based on changing ω_r of the phase shifter by tuning the resonance capacitors. Interestingly as (23) suggests, an optimum K results in maximum change of ω with respect to ω_r.

Fig. 12 shows the simulated phase shift for each phase shifter at ω_0 as a function of the control voltage. Note that the actual phase shift is determined by the locking frequency that is slightly different from ω_0. The resulting change in the locking frequency of the oscillators is also shown in Fig. 12. The control voltage used in this plot is the DC voltage across the varactors. Since the gate of all varactors are biased at 1.2 V, all voltages are positive in the entire range.

In practice K also changes both with respect to the control voltage and the frequency. For an accurate picture of the frequency tuning, one also has to consider the change in the gain of the coupling amplifiers. However, in this design most of the frequency tuning is achieved within the voltage range where the coupling amplitude can be considered constant.

IV. Implementation

The coupled oscillator VCO is designed and implemented in a 65 nm low-power (LP) bulk CMOS process. The chip photo is shown in Fig. 13. This section discusses the steps taken for proper modeling and simulation of the VCO, followed by the measurement setup and the measured results.

A. Simulation

Proper simulation of all connections and couplings are crucial in this design. This is particularly important in the core oscillators where the matching and power combining networks operate around 300 GHz and all lines are comparable with the wavelength. The core is designed based on the design methodology described in Section III. First, the center frequency is set by l_d and Z_d of the drain transmission line. Next, harmonic matching is achieved by tuning l_g and Z_g of the gate transmission line. We use shielded RF devices with a finger width of 2 μm both for the core and the coupling circuits. The width of the transistors in the core oscillator is 36 μm. The sizes of M1, M2, and M3 in the coupling block of Fig. 11 are 12 μm, 24 μm, and 24 μm, respectively.

Ground shielding is placed under all transmission lines by using the first and second metal layers in parallel. Fig. 14 shows the structure used for the transmission lines. Because of the proximity between the gate and drain lines, the effect of coupling between the lines should be simulated. In order to do so, the entire metallization of the core oscillator is modeled as a 5-port device, four connected to the gates and drains of the cross-coupled pair and one connecting the output to the combining network. A symmetric layout is vital for maximizing the fourth harmonic power generation and canceling lower harmonics. Each core oscillator is shielded from other blocks using grounded metal walls.

The differential coupling block is designed to achieve equal lengths for the two differential signal paths. To achieve a fully differential scheme, the inductors of the phase shifter are designed to be differential and their common node is wirebonded to the DC supply. The varactors in the phase shifters are buffered from the cores and as a result, they have minimal effect on the quality factor of the oscillators. All varactors are connected to bypass capacitors and are ESD protected prior to connecting to the pads. The phase shifters are designed to achieve good phase tuning and sufficient energy coupling at the same time. The front-end buffer device, M1 is smaller that the next two stages in order to minimize the loading effect of the coupling circuit on the injecting oscillator. The power combiner is designed for matching at the fourth harmonic frequency as shown in Fig. 9. Since the reactance of the pad capacitance is significant at the target frequency, its effect is considered in designing the combiner network.

B. Measurement

We use two separate setups to measure the output frequency and power. These two test setups are shown in Fig. 15. The

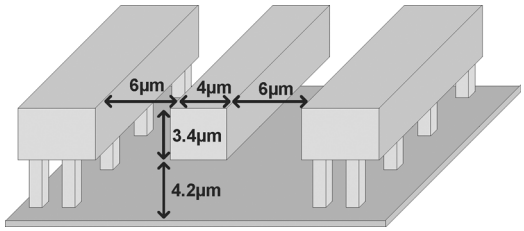

Fig. 14. Metal layers and the dimensions of transmission lines.

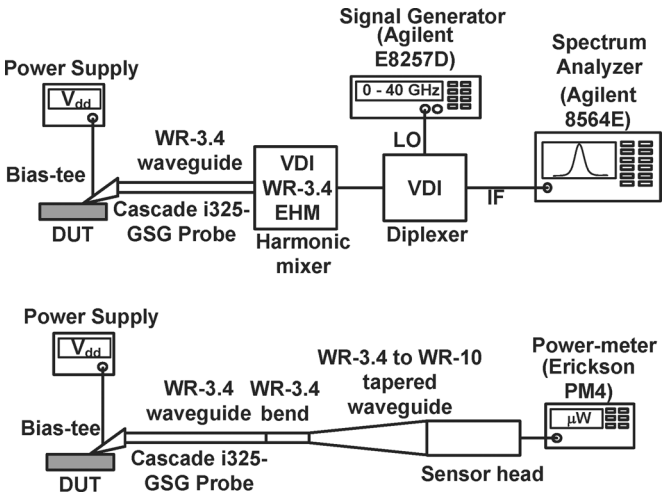

Fig. 15. Top: Test setup for measuring the output frequency. Bottom: Test setup for measuring the output power.

output of the VCO is connected to a Cascade i325-GSG probe with a built-in bias tee that provides the DC current to the four cores. An alternative to using a bias tee is to provide the DC current using wirebonds and use a quarter wavelength stub to connect the supply to the output node. To measure the output frequency, a VDI WR3.4EHM harmonic mixer is used for down-converting the sub-mm-wave signal. The LO is set so that the down-converted IF is below 1 GHz. In order to calculate the output frequency, we first find the harmonic number of the LO which is multiplied with the RF signal. This is done by changing LO and finding the ratio between the frequency change in IF with respect to the frequency change in LO. Fig. 16 shows the IF spectrum from the 16th harmonic of the LO.

By selecting two different values for the drain inductor L_d, two versions of the chip are designed at two different center frequencies. Figs. 17 and 18 show the measured output frequency for the two VCOs as a function of the control voltage. The first VCO has around 13 GHz of tuning range around 290 GHz while the second VCO has a tuning range of 8.4 GHz around 320 GHz. The second VCO has a lower tuning range because the coupling circuit for both versions are the same, while the tuning range of the phase shifter is centered around 290 GHz. As shown in Fig. 12, the tuning range of the phase shifter is less than 180 degrees, thus, the frequency tuning range can be further increased by adding another stage to the phase shifter.

For output power measurement, a wide-band Erikson PM4 power meter is employed. As shown in Fig. 15, the probe is connected to a 90 degree bend which is followed by a WR3.4

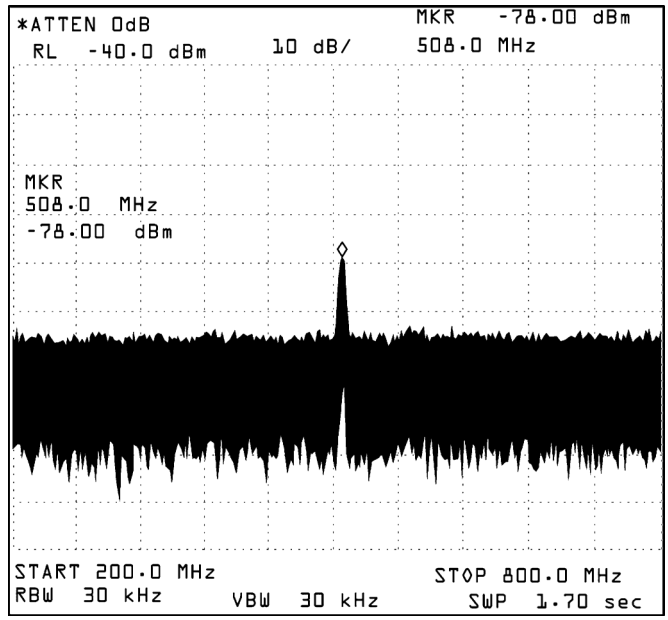

Fig. 16. A typical measured output spectrum downconverted by the 16th harmonic of the LO.

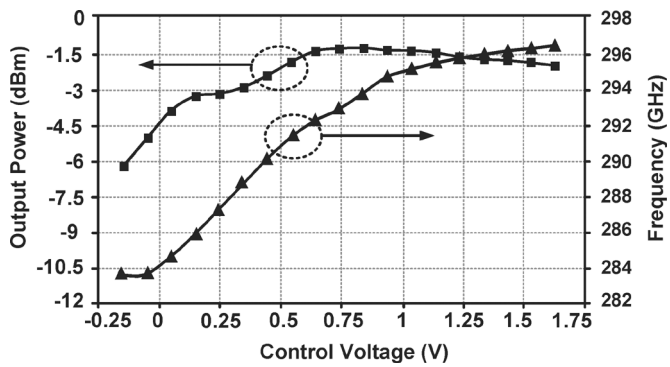

Fig. 17. Measured output power and frequency tuning for the 290 GHz VCO.

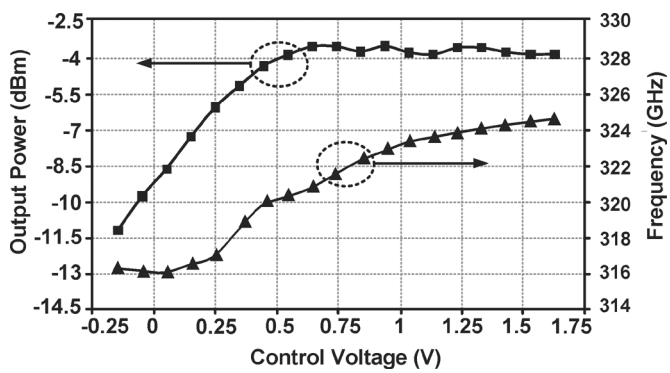

Fig. 18. Measured output power and frequency tuning for the 320 GHz VCO.

to WR10 tapered line. The loss of all the components are calibrated using a 500 GHz network analyzer. Fig. 19 shows the peak output power as a function of the input DC power to the cores. The design point for both chips is chosen at the point with the best DC to THz power efficiency. Figs. 17 and 18 show the output power as a function of the control voltage. The variation in the output power is mostly due to variation in the gain of the

TABLE I
PERFORMANCE COMPARISON OF THE STATE-OF-THE-ART TERAHERTZ SIGNAL SOURCES

Ref.	Frequency (GHz)	Output Power (dBm)	Tuning Range	Phase Noise (dBc/Hz)	DC Power (mW)	DC to THz Efficiency	Technology	Source Type
This Work	290	-1.2	4.5%	-78 @ 1 MHz	325	0.23%	65 nm LP Bulk CMOS	Oscillator
This Work	320	-3.3	2.6%	-77 @ 1 MHz	339	0.13%	65 nm LP Bulk CMOS	Oscillator
[13]	482	-7.9	Non-tunable	-76 @ 1 MHz	61	0.26%	65 nm Bulk CMOS	Oscillator
[14]	291	-13.9 (*)	Non-tunable	NA	19	0.21%	45 nm SOI CMOS	Oscillator
[15]	324	-46	1.2%	-78 @ 1 MHz	12	0.0002%	90 nm Bulk CMOS	Oscillator
[18]	296	-3.9	4%	-78 @ 1 MHz	115	0.35%	InP HBT $f_{max} > 800GHz$	Oscillator
[19]	190	0	13.6%	NA	91	1.1%	45 nm SOI CMOS	Frequency Multiplier
[21]	325	-3	6.2%	-101 (**) @ 1 MHz	420	0.12%	130 nm SiGe HBT	Frequency Multiplier

(*) Generated power from each oscillator assuming antenna efficiency of 50%.

(**) Employs a high-power low-noise external source.

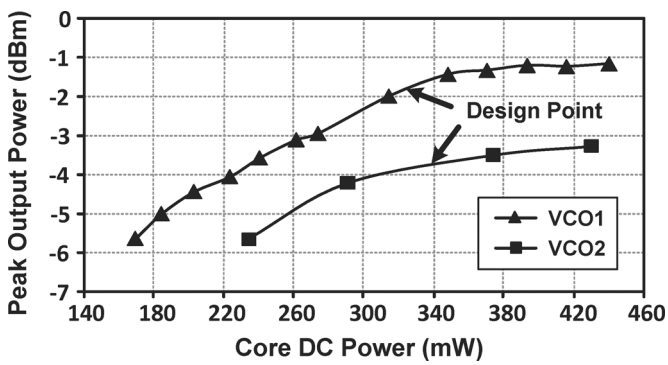

Fig. 19. Measured peak output power vs. DC power.

phase shifters for different control voltages. Although the oscillator systematically cancels all the lower harmonics, mismatch between cores can lead to some undesired harmonic leakage to the output. However, the amount of this leaked output power is small compared to the main harmonic. Any leaked power is largely filtered out by the output matching network and the high-pass nature of the rectangular waveguides. This is verified by observing the output spectrum of the lower harmonics, which are at least 15 dB lower than the fourth harmonic.

For the first VCO, the peak output power is -1.2 dBm and the tuning range is 4.5% around 290 GHz. The second VCO has a peak output power of -3.3 dBm with a 2.6% tuning range around 320 GHz. The measured phase noises of the 290 GHz and 320 GHz sources at the 1 MHz offset frequency are -78 dBc/Hz and -77 dBc/Hz, respectively. Each oscillator core consumes 81 mW from a 1.3 V supply voltage and the power consumption of each coupling block is 31 mW from a 1.1 V supply voltage. Because of the large DC current flowing into the cores, the supply of the core oscillators is slightly higher than the nominal value of 1.2 V in order to compensate for the voltage drop from the pad to the drain of the transistors.

Table I compares the performance of this VCO with the best signal sources around 300 GHz. Prior to this work, the highest output powers on CMOS were achieved with non-tunable oscillators. This VCO achieves both the highest output power and the highest tunability compared to all the oscillators including compound semiconductors technologies that have significantly higher cut-off frequencies. The DC to THz conversion efficiency of this work is more than any other CMOS tunable source at this frequency range. However, this efficiency is still below 1%. This is mainly because a large portion of the DC power is converted to the fundamental frequency as well as undesirable harmonics. It is intriguing to explore novel harmonic generation schemes to maximize the conversion from DC to the desired harmonic by minimizing undesired harmonic generation.

V. CONCLUSION

In this work, we propose a novel oscillator architecture that is suitable for high-power generation in the terahertz region. The coupled oscillator structure introduces a unique power generation and combining method that produces high harmonic power above the transistor $f_{\max}$. As a result of this architecture, power

generation and tuning can be performed without affecting each other. The measured output power and tuning range of this VCO is the highest compared to CMOS VCOs at this range and is comparable to compound semiconductor oscillators with much higher $f_{\max}$.

ACKNOWLEDGMENT

The authors thank the TSMC University Shuttle Program for chip fabrication and Sonnet for software support. They also acknowledge the support of the C2S2 Focus Center under FCRP, an SRC entity, and the National Science Foundation.

REFERENCES

[1] C. Marcu, D. Chowdhury, C. Thakkar, J. Park, L. Kong, M. Tabesh, Y. Wang, B. Afshar, A. Gupta, A. Arbabian, S. Gambini, R. Zamani, E. Alon, and A. M. Niknejad, "A 90 nm CMOS low-power 60 GHz transceiver with integrated baseband circuitry," *IEEE J. Solid-State Circuits*, vol. 44, no. 12, pp. 3434–3447, Dec. 2009.

[2] J. Lee, Y. Chen, and Y. Huang, "A low-power low-cost fully-integrated 60-GHz transceiver system with OOK modulation abd on-board antenna assembly," *IEEE J. Solid-State Circuits*, vol. 45, no. 2, pp. 264–275, Feb. 2010.

[3] T. Mitomo, N. Ono, H. Hoshino, Y. Yoshihara, O. Watanabe, and I. Seto, "A 77 GHz 90 nm CMOS transceiver for FMCW radar applications," *IEEE J. Solid-State Circuits*, vol. 45, no. 4, pp. 928–937, Apr. 2010.

[4] A. Arbabian, S. Callender, S. Kang, B. Afshar, J. Chien, and A. M. Niknejad, "A 90 GHz hybrid switching pulse-transmitter for medical imaging," *IEEE J. Solid-State Circuits*, vol. 45, no. 12, pp. 2667–2681, Dec. 2010.

[5] I. Sarkas, S. T. Nicolson, A. Tomkins, E. Laskin, P. Chevalier, B. Sautreuil, and S. P. Voinigescu, "An 18-Gb/s, direct QPSK modulation SiGe BiCMOS transceiver for last mile links in the 70–80 GHz band," *IEEE J. Solid-State Circuits*, vol. 45, no. 10, pp. 1968–1980, Oct. 2010.

[6] A. Natarajan, S. K. Reynolds, M. Tsai, A. T. Nicolson, J. C. Zhan, D. G. Kam, D. Liu, Y. O. Huang, A. Valdes-Garcia, and B. A. Floyd, "A fully-integrated 16-element phased-array receiver in SiGe BiCMOS for 60-GHz communications," *IEEE J. Solid-State Circuits*, vol. 46, no. 5, pp. 1059–1075, May 2011.

[7] A. Tomkins, P. Garcia, and S. P. Voinigescu, "A passive W-band imaging receiver in 65-nm bulk CMOS," *IEEE J. Solid-State Circuits*, vol. 45, no. 10, pp. 1981–1991, Oct. 2011.

[8] L. Gilreath, V. Jain, and P. Heydari, "Design and analysis of a W-band SiGe direct-detection-based passive imaging receiver," *IEEE J. Solid-State Circuits*, vol. 46, no. 10, pp. 2240–2252, Oct. 2011.

[9] S. Koch, M. Guthoerl, I. Kallfass, A. Leuther, and S. Saito, "A 120–145 GHz heterodyne receiver chipset utilizing the 140 GHz atmospheric window for passive millimeter-wave imaging applications," *IEEE J. Solid-State Circuits*, vol. 45, no. 10, pp. 1961–1967, Oct. 2010.

[10] A. Tang and M. F. Chang, "183 GHz 13.5 mW/pixel CMOS regenerative receiver for mm-wave imaging applications," in *IEEE ISSCC Dig. Tech. Papers*, 2011, pp. 296–298.

[11] H. Sherry, J. Grzyb, Y. Zhao, R. Al Hadi, A. Cathelin, A. Kaiser, and U. Pfeiffer, "A 1 kPixel CMOS camera chip for 25 FPS real-time terahertz imaging applications," in *IEEE ISSCC Dig. Tech. Papers*, 2012, pp. 252–254.

[12] R. Han, Y. Zhang, Y. Kim, D. Kim, H. Shichijo, E. Ahshari, and K. K. O, "280 GHz and 860 GHz image sensors using Schottky-barrier diodes in 0.13 μm digital CMOS," in *IEEE ISSCC Dig. Tech. Papers*, 2012, pp. 254–256.

[13] O. Momeni and E. Afshari, "High power terahertz and millimiter-wave oscillator design: A systematic approach," *IEEE J. Solid-State Circuits*, vol. 46, no. 3, pp. 583–597, Aug. 2010.

[14] K. Sengupta and A. Hajimiri, "Distributed active radiation for THz signal generation," in *IEEE ISSCC Dig. Tech. Papers*, 2011, pp. 288–289.

[15] D. Huang, T. R. LaRocca, M. F. Chang, L. Samoska, A. Fung, R. L. Campbell, and M. Andrews, "Terahertz CMOS frequency generator using linear superposition technique," *IEEE J. Solid-State Circuits*, vol. 43, no. 12, pp. 2730–2738, Dec. 2010.

[16] E. Seok, D. Shim, C. Mao, R. Han, S. Sankaran, C. Cao, W. Knap, and K. K. O, "Progress and challenges towards terahertz CMOS integrated circuits," *IEEE J. Solid-State Circuits*, vol. 45, no. 8, pp. 1554–1564, Aug. 2010.

[17] B. Razavi, "A 300-GHz fundumental oscillator in 65-nm CMOS technology," *IEEE J. Solid-State Circuits*, vol. 46, no. 4, pp. 894–903, Apr. 2011.

[18] M. Seo, M. Urteaga, J. Hacker, A. Young, Z. Griffith, V. Jain, R. Pierson, P. Rowell, A. Skalare, A. Peralta, R. Lin, D. Pukala, and M. Rodwell, "InP HBT IC technology for terahertz frequencies: Fundamental oscillators up to 0.57 THz," *IEEE J. Solid-State Circuits*, vol. 46, no. 10, pp. 2203–2214, Oct. 2011.

[19] A. Cetinoneri, Y. A. Atesl, A. Fung, and G. M. Rabeiz, "W-band amplifiers with 6 dB noise figure and mW-level 170–200 GHz doublers in 45-nm CMOS," *IEEE Trans. Microw. Theory Tech.*, vol. 60, no. 3, pp. 692–701, Mar. 2011.

[20] O. Momeni and E. Afshari, "A 220-to-275 GHz traveling-wave frequency doubler with -6.6 dBm power at 244 GHz in 65 nm CMOS," in *IEEE ISSCC Dig. Tech. Papers*, 2011, pp. 286–288.

[21] E. Ojefors, B. Heinemann, and U. R. Pfeiffer, "Active 220- and 325-GHz frequency multiplier chains in an SiGe HBT technology," *IEEE Trans. Microw. Theory Tech.*, vol. 59, no. 5, pp. 1311–1318, May 2011.

[22] G. Cusmai, M. Repossi, G. Albasini, A. Mazzanti, and F. Svelto, "A magnetically tuned quadrature oscillator," *IEEE J. Solid-State Circuits*, vol. 42, no. 12, pp. 2870–2877, Dec. 2007.

[23] K. Kwok and J. R. Long, "A 23-to-29 GHz transconductor-tuned VCO MMIC in 0.13 μm CMOS," *IEEE J. Solid-State Circuits*, vol. 42, no. 12, pp. 2878–2886, Dec. 2007.

[24] G. Li, L. Liu, Y. Tang, and E. Afshari, "A low-phase-noise wide-tuning-range oscillator based on resonant mode switching," *IEEE J. Solid-State Circuits*, vol. 47, no. 6, pp. 1295–1308, Jun. 2012.

[25] S. Rong and H. C. Luong, "Design and analysis of varactor-less interpolative-phase-tuning millimiter-wave LC oscillators with multiphase outputs," *IEEE J. Solid-State Circuits*, vol. 46, no. 8, pp. 1810–1819, Aug. 2011.

[26] Y. M. Tousi, O. Momeni, and E. Afshari, "A 283-to-296 GHz VCO with 0.76 mW peak output power in 65 nm CMOS," in *IEEE ISSCC Dig. Tech. Papers*, 2012, pp. 258–256.

[27] R. Adler, "Study of locking phenomena in oscillator," in *Proc. IRE*, Jun. 1946, vol. 34, pp. 351–357.

[28] B. Razavi, "A study of injection locking and pulling in oscillators," *IEEE J. Solid-State Circuits*, vol. 39, no. 9, pp. 1415–1424, Sep. 2004.

[29] B. Lin and S. Liu, "Analysis and design of D-band injection-locked frequency dividers," *IEEE J. Solid-State Circuits*, vol. 46, no. 6, pp. 1250–1264, Jun. 2011.

[30] J. F. Buckwalter, A. Babakhani, A. Komijani, and A. Hajimiri, "An integrated subharmonic coupled-oscillator scheme for a 60-GHz phased-array transmitter," *IEEE Trans. Microw. Theory Tech.*, vol. 54, no. 12, pp. 4271–4280, Dec. 2006.

[31] P. Liao and R. A. York, "A new phase-shifterless beam-scanning technique using arrays of coupled oscillators," *IEEE Trans. Microw. Theory Tech.*, vol. 41, no. 10, pp. 1810–1815, Oct. 1993.

[32] J. J. Lynch and R. A. York, "Synchronization of oscillators coupled through narrow-band networks," *IEEE Trans. Microw. Theory Tech.*, vol. 49, no. 2, pp. 237–249, Feb. 2001.

[33] R. A. York, "Nonlinear analysis of phase relationships in quasi-optical oscillator arrays," *IEEE Trans. Microw. Theory Tech.*, vol. 41, no. 10, pp. 1799–1809, Oct. 1993.

[34] H. Chang, X. Cao, M. J. Vaughan, U. K. Mishra, and R. A. York, "Phase noise in externally injection-locked oscillator arrays," *IEEE Trans. Microw. Theory Tech.*, vol. 45, no. 11, pp. 2035–2042, Nov. 1997.

[35] R. A. York and R. C. Compton, "Quasi-optical power combining using mutually synchronized oscillator arrays," *IEEE Trans. Microw. Theory Tech.*, vol. 39, no. 6, pp. 1000–1009, Jun. 1991.

[36] Y. M. Tousi, V. Pourahmad, and E. Afshari, "Delay coupled oscillators for frequency tuning of solid-state terahertz sources," *Phys. Rev. Lett.*, vol. 108, no. 23, Jun. 2012.

[37] S. H. Strogatz, *Nonlinear Dynamics and Chaos With Applications to Physics, Biology, Chemisty, and Engineering*. Boston, MA: Addison-Wesley, 1998.

[38] S. Li, I. Kipnis, and M. Ismail, "A 10-GHz CMOS quadrature LC-VCO for multirate optical applications," *IEEE J. Solid-State Circuits*, vol. 38, no. 10, pp. 1626–1634, Oct. 2003.

[39] D. M. Pozar, *Microwave Engineering*, 3rd ed. Hoboken, NJ: Wiley, 2005.

Yahya Mesgarpour Tousi (M'12) received the B.S. degree in 2004 and the M.S. degree in 2006, both in electrical engineering, from Sharif University of Technology, Tehran, Iran. In 2007 he joined Cornell University, Ithaca, NY, to pursue the Ph.D. degree in electrical engineering.

During summer 2010, he was with SiTune Corporation where he worked on the RF front-end for TV tuners. He is interested in novel high-speed integrated circuits and systems for communication, biomedical, and signal processing applications.

Mr. Tousi is the recipient of the 2009 Cornell Jacob Fellowship, and the 2011 IEEE Microwave Theory and Techniques Society Graduate Fellowship. He is also the winner of the Graduate Research Competition at IMS 2011, and the recipient of the 2011–2012 IEEE Solid-State Circuits Society Pre-Doctoral Achievement Award.

Omeed Momeni (M'11) received the B.Sc. degree from Isfahan University of Technology, Isfahan, Iran, the M.S. degree from University of Southern California, Los Angeles, CA, and the Ph.D. degree from Cornell University, Ithaca, NY, all in electrical engineering, in 2002, 2006, and 2011, respectively.

He joined the faculty of Electrical and Computer Engineering Department at University of California, Davis in 2011. He was a visiting Professor in the Electrical Engineering and Computer Science Department at the University of California, Irvine, from 2011 to 2012. From 2004 to 2006, he was with the National Aeronautics and Space Administration (NASA), Jet Propulsion Laboratory (JPL), to design L-band transceivers for synthetic aperture radars (SAR) and high power amplifiers for mass spectrometer applications. His research interests include mm-wave and terahertz integrated circuits and systems.

Prof. Momeni is the recipient of the Best Ph.D. Thesis Award from the Cornell ECE Department in 2011, the Outstanding Graduate Award from Association of Professors and Scholars of Iranian Heritage (APSIH) in 2011, the Best Student Paper Award at the IEEE Workshop on Microwave Passive Circuits and Filters in 2010, the Cornell University Jacob's fellowship in 2007 and the NASA-JPL fellowship in 2003.

Ehsan Afshari (M'07–SM'11) was born in 1979. He received the B.Sc. degree in electronics engineering from Sharif University of Technology, Tehran, Iran, and the M.S. and Ph.D. degree in electrical engineering from the California Institute of Technology, Pasadena, in 2003, and 2006, respectively.

In August 2006, he joined the faculty of Electrical and Computer Engineering at Cornell University, Ithaca, NY. His research interests are mm-wave and terahertz electronics and low-noise integrated circuits for applications in communication systems, sensing, and biomedical devices.

Prof. Afshari serves as the chair of the IEEE Ithaca section, as the chair of Cornell Highly Integrated Physical Systems (CHIPS), as a member of International Technical Committee of the IEEE Solid-State Circuit Conference (ISSCC), as a member of the Analog Signal Processing Technical Committee of the IEEE Circuits and Systems Society, as a member of the Technical Program Committee of the IEEE Custom Integrated Circuits Conference (CICC), and as a member of Technical Program Committee of the IEEE International Conference on Ultra-Wideband (ICUWB). He was awarded the National Science Foundation CAREER award in 2010, the Cornell College of Engineering Michael Tien excellence in teaching award in 2010, the Defense Advanced Research Projects Agency (DARPA) Young Faculty Award in 2008, and Iran's Best Engineering Student Award by the President of Iran in 2001. He is also the recipient of the best paper award in the Custom Integrated Circuits Conference (CICC), September 2003, the first place at Stanford-Berkeley-Caltech Inventors Challenge, March 2005, the best undergraduate paper award in Iranian Conference on Electrical Engineering, 1999, the recipient of the Silver Medal in the Physics Olympiad in 1997, and the recipient of the Award of Excellence in Engineering Education from Association of Professors and Scholars of Iranian Heritage (APSIH), May 2004.